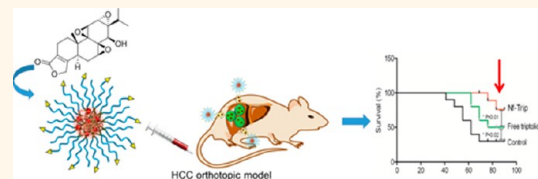


# pH-Sensitive Nanoformulated Triptolide as a Targeted Therapeutic Strategy for Hepatocellular Carcinoma

Daishun Ling,<sup>†,‡,||</sup> Hongping Xia,<sup>§,||</sup> Wooram Park,<sup>†</sup> Michael J. Hackett,<sup>†,‡</sup> Changyeong Song,<sup>†,‡</sup> Kun Na,<sup>†</sup> Kam Man Hui,<sup>§,\*</sup> and Taeghwan Hyeon<sup>†,‡,\*</sup>

<sup>†</sup>Center for Nanoparticle Research, Institute for Basic Science (IBS), Seoul 151-742, Korea, <sup>‡</sup>School of Chemical and Biological Engineering, Seoul National University, Seoul 151-742, Korea, <sup>§</sup>Laboratory of Cancer Genomics, Division of Cellular and Molecular Research, Humphrey Oei Institute of Cancer Research, National Cancer Center Singapore, Cancer and Stem Cell Biology Program, Duke-NUS Graduate Medical School, Department of Biochemistry, Yong Loo Lin School of Medicine, National University of Singapore, Institute of Molecular and Cell Biology, A\*STAR, Biopolis Drive Proteos, Singapore 169610, and <sup>||</sup>Department of Biotechnology, The Catholic University of Korea, Bucheon-si, Gyeonggi-do 420-743, Korea. <sup>||</sup>These authors contributed equally to this work.

**ABSTRACT** Hepatocellular carcinoma (HCC) has one of the worst prognoses for survival as it is poorly responsive to both conventional chemotherapy and mechanism-directed therapy. This results from a lack of therapeutic concentration in the tumor tissue coupled with the highly toxic off-site effects exhibited by these compounds. Consequently, we believe the best packaging for holistic therapy for HCC will involve three components: a potent therapeutic, a rationally designed drug delivery vehicle to enrich the target site concentration of the drug, and a surface ligand that can enable a greater propensity to internalization by tumor cells compared to the parenchyma. We screened a library containing hundreds of compounds against a panel of HCC cells and found the natural product, triptolide, to be more effective than sorafenib, doxorubicin, and daunorubicin, which are the current standards of therapy. However, the potential clinical application of triptolide is limited due to its poor solubility and high toxicity. Consequently, we synthesized tumor pH-sensitive nanoformulated triptolide coated with folate for use in an HCC-subpopulation that overexpresses the folate receptor. Our results show triptolide itself can prevent disease progression, but at the cost of significant toxicity. Conversely, our pH-sensitive nanoformulated triptolide facilitates uptake into the tumor, and specifically tumor cells, leading to a further increase in efficacy while mitigating systemic toxicity.



**KEYWORDS:** hepatocellular carcinoma · triptolide · pH sensitive polymer · targeted cancer therapy · drug delivery

Hepatocellular carcinoma (HCC) is the most common form of primary liver cancer and second leading cause of cancer-associated death worldwide.<sup>1</sup> The clinical management of advanced and metastatic HCC is challenging on many counts. Unfortunately, at diagnosis less than 30% of patients are deemed eligible for curative interventions including surgical resection, liver transplantation, and chemoembolization. Moreover, conventional chemotherapeutic drugs such as doxorubicin have not been shown to significantly extend the survival of the patients with inoperable HCC.<sup>2</sup> Other conventional chemotherapeutic agents such as epirubicin, cisplatin, 5-fluorouracil, etoposide, and combinations therein were found to have even lower efficacy than doxorubicin alone.<sup>3</sup> Consequently, the overall prognosis of patients with advanced HCC is dismal. Recently, personalized target therapy has

become an important strategy in the management of patients with advanced stage cancer including HCC.<sup>4</sup> Many ongoing clinical trials aim to improve the treatment of HCC by targeting specific subpopulations of patients. In 2007, sorafenib, an oral multi-kinase inhibitor, was approved by the FDA as a first-line treatment for advanced HCC, but the treatment only increased progression-free survival by a paltry two months compared to placebo.<sup>5,6</sup> Meanwhile, over 80% of phase 3 trials for targeted molecular therapies within the last five years have failed to prolong survival of patients with advanced disease.<sup>4</sup> Therefore, the dismal prognosis for most HCC patients underscores an urgent need to discover and develop more effective therapeutic strategies against HCC.

Triptolide, a diterpenoid triepoxide isolated from the plant *Tripterygium wilfordii*, is a natural product that has already been

\* Address correspondence to  
thyeon@snu.ac.kr,  
cmrhkm@nccs.com.sg.

Received for review April 14, 2014  
and accepted July 29, 2014.

Published online August 05, 2014  
10.1021/nn502074x

© 2014 American Chemical Society

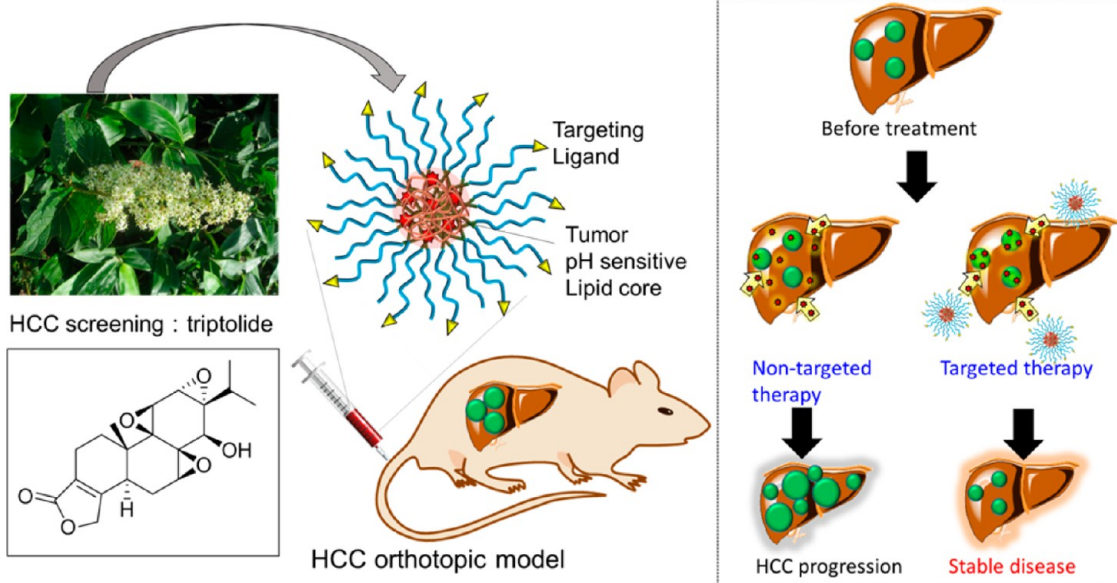


**Figure 1.** Schematic representation of tumor-responsive nanoformulated triptolide (Nf-Trip) for Hepatocellular Carcinoma (HCC) targeted therapy.

found to be highly effective against many malignant cancer types including pancreatic cancer,<sup>7,8</sup> neuroblastoma,<sup>9</sup> and cholangiocarcinoma.<sup>10</sup> Although triptolide was initially considered by many to be a promising chemotherapeutic agent, its potential clinical application has been limited due to its poor solubility and extremely high toxicity.<sup>11</sup> Recently, a synthetic prodrug of triptolide called minnelide has been studied preclinically as a therapeutic agent against pancreatic cancer.<sup>12</sup> Minnelide has a methylphosphate moiety synthesized on the secondary alcohol of triptolide to affect greater solubility and provide a site for rapid dephosphorylation by the ubiquitous enzyme alkaline phosphatase. While this prodrug does exhibit an increase in solubility and serum half-life, it is not delivered specifically to tumor cells which limits its efficacy.<sup>12</sup>

Nanotechnology-based drug delivery systems have been shown to improve tumoral drug accumulation and reduce toxicity.<sup>13–16</sup> Multifunctional nanoparticles<sup>17–21</sup> are emerging as the next-generation anticancer agents.<sup>22–28</sup> Due to heavy bloodflow and fenestrated endothelia, intravenously injected nanoparticles are generally taken up by the liver.<sup>29</sup> This process may be more pronounced in the case of liver cancer due to local enhanced permeability and retention (EPR) effect.<sup>30</sup> Furthermore, nanoparticles can be designed to be responsive to the local tumor microenvironment or to tissue-specific interactions with selectively overexpressed receptors in tumors.<sup>13,15</sup> This can include “active targeting” of tumor cells through surface receptors (e.g., folate receptor)<sup>31–33</sup> or drug release triggered by locally expressed enzymes.<sup>13–15</sup> Additionally, the extracellular pH of solid tumors is more acidic (pH ~6.8) in comparison to normal tissue,<sup>34–36</sup> and the endolysosomes of cancer cells are even more acidic (pH < 6).<sup>37</sup>

Thus, the utilization of the differential in tumor pH can be considered a robust and simple strategy to achieve broad tumor applicability.<sup>38–40</sup> Herein, we report on the designed synthesis of a tumor-responsive nanoformulated triptolide (Nf-Trip) for HCC targeted therapy (Figure 1).

## RESULTS AND DISCUSSION

**Development and Characterization of Nanoformulated Triptolide (Nf-Trip).** Triptolide was initially selected due to its efficacy across a variety of liver cancer cell lines (Figure S1a in the Supporting Information). When compared to the more commonly utilized clinical chemotherapies for HCC patients (sorafenib, doxorubicin, and daunorubicin), triptolide again induced much stronger cytotoxic effects across the panel of human liver cancer cell lines (Figure S1b–e in the Supporting Information). This corroborates well with several recent reports demonstrating that triptolide is a strong cytotoxic agent in human HCC cell lines and increased cellular sensitivity to combination therapies of cisplatin and 5-FU.<sup>41,42</sup> To assess the effect of triptolide on cell death in liver cancer cell lines, two liver cancer cell lines, Bel-7404 and HCCLM3, were treated with triptolide at a concentration of 10 ng/mL. As expected, triptolide treatment induced significant effects on cell death in both liver cancer cell lines. The cell lines were assessed by Annexin-V and 7-AAD analysis using flow cytometry. The results showed that both Annexin-V positive and 7-AAD positive cells were significantly increased in both Bel-7404 and HCCLM3 cells within 24 h of treatment at 10 ng/mL triptolide, indicating substantial amounts of apoptosis and necrosis (Figure S2 in the Supporting Information).

Since the potential clinical application of triptolide has been limited due to its poor solubility and extremely

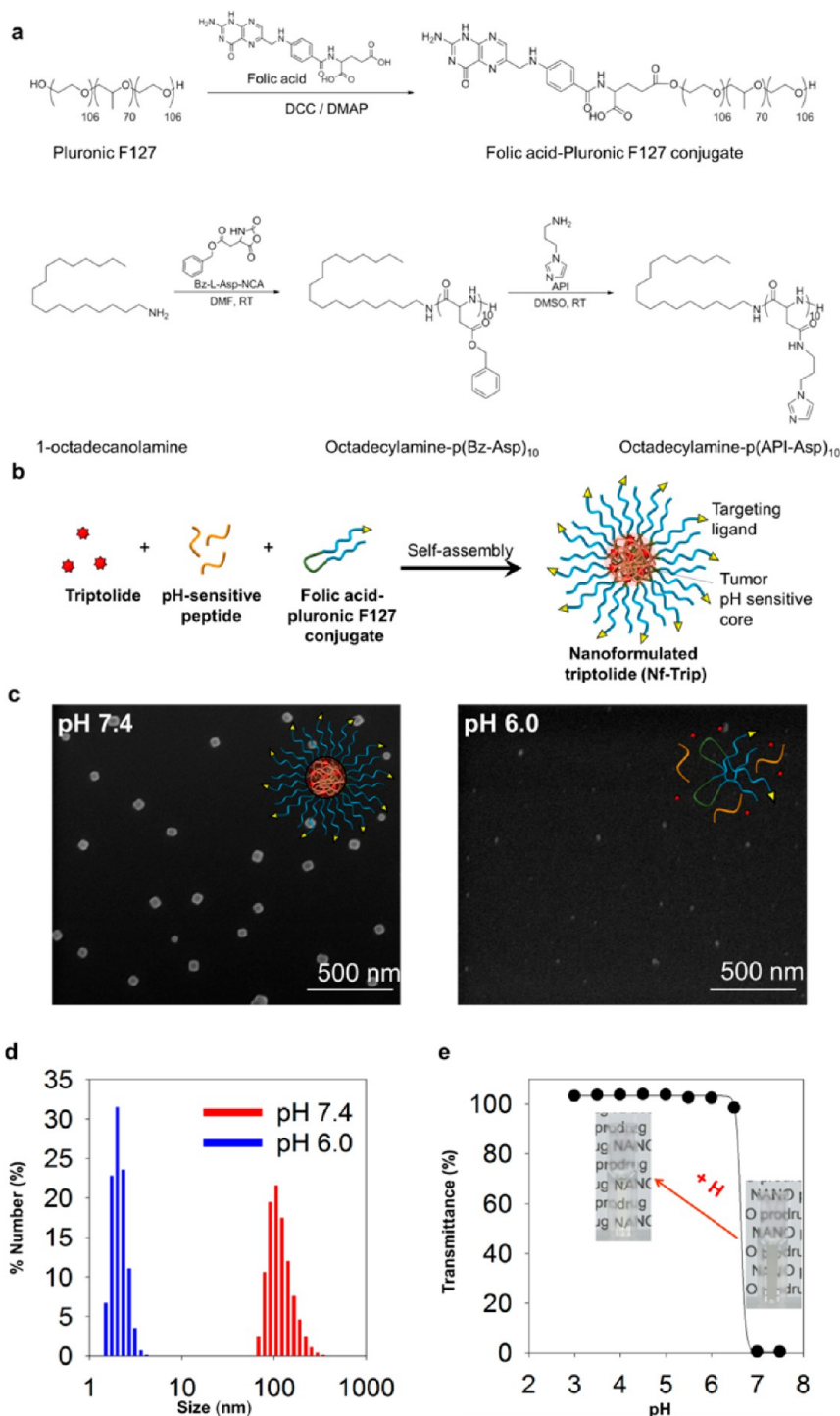


**Figure 2.** Synthesis and characterization of nanoformulated triptolide (Nf-Trip). (a) Synthetic scheme of the pluronic F127-folate conjugate and octadecylamine-p(API-Asp)<sub>10</sub>. (b) Fabrication of Nf-Trip through self-assembly. (c) SEM images of Nf-Trip at pH 7.4 and pH 6.0. (d) DLS size measurement of Nf-Trip (0.1 mg/mL) as a function of pH. (e) Percent transmittance of an Nf-Trip suspension as a function of pH. The inset photo presents data for pH-dependent turbidity of the Nf-Trip solution as shown by legibility of the background.

high toxicity,<sup>11</sup> the drug was packaged into a tumor pH-sensitive nanogel coated with folate for targeting an HCC-subpopulation that overexpresses the folate receptor. Nf-Trip is composed of natural triptolide and two polymers synthesized from generally recognized as safe (GRAS) materials. One polymer is pluronic F127

esterified with folic acid (Figure 2a and Figure S3 in the Supporting Information) and the other is a synthetic 10-mer of aspartic acid with an octadecylamine tail and ionizable imidazole side chains for pH sensitivity (Figure 2a and Figure S4 in the Supporting Information). Our unique pH-sensitive polymer design has two

advantages. First, it was synthesized through facile two-step reactions: (1) ring opening polymerization (ROP) of  $\alpha$ -amino acid *N*-carboxyanhydrides (NCAs) using octadecylamine as an initiator and (2) introduction of pH-responsive ionizable groups (e.g., imidazole groups) through an aminolysis reaction; such simple procedure could facilitate the clinical translation of cancer nanotechnology. Second, the use of octadecylamine as an initiator for ROP further provides a superhydrophobic moiety to the resulting pH sensitive polypeptide, which facilitates the high loading efficiency of a hydrophobic drug such as triptolide.

The polymers spontaneously form a micelle structured nanogel in water (Figure 2b). The surface exposed folate acts as a cancer cell-targeting ligand,<sup>31–33</sup> while the internally packed imidazoles provide an ionizable moiety for pH-sensitive ionization and dispersion (Figure 2c–e).<sup>33,43,44</sup> Folate was selected as the targeting ligand due to the high expression levels of folate receptor of our clinical HCC samples (Figure S5 in the Supporting Information). Triptolide was loaded into the hydrophobic core of the nanogel by thin-film hydration. The as-synthesized polymers and triptolide were dissolved in methanol and then dried into a film on the walls of round-bottom flask. Phosphate buffered saline (PBS, pH 7.4) was subsequently added to the flask to hydrate the film followed by stirring and ultrasonication yielding a stable nanogel. To remove unloaded drug, the sample was dialyzed against PBS for 12 h. The resulting Nf-Trip has a drug-to-carrier ratio of ~9% (w/w) and a high loading efficiency of ~94% (Figure S6 in the Supporting Information). The hydrodynamic radius of the resulting Nf-Trip at physiological pH was measured to be ~120 nm (Figure 2d). The acid-sensitivity of the Nf-Trip was first examined by scanning electron microscopy (SEM) and dynamic light scattering (DLS). At physiological pH, distinct nanoparticles are observed, but upon acidification to pH 6.0, the nanoparticles completely collapsed (Figure 2c,d). Acid–base titration (Figure 2e) also demonstrated a stepwise drop in % transmittance at the critical pH range of ~6.5. It should be noted that Nf-Trip's particle morphology is retained at pH 6.8 (Figure S7 in the Supporting Information), suggesting Nf-Trip should retain its cell targeting functionality for receptor-mediated internalization of nanoparticles at the tumor microenvironment (pH = ~6.8). By developing Nf-Trip, we were able to solubilize the drug for intravenous administration and take advantage of the size-dependent accumulation of the nanoparticles in inflamed tumoral tissues *via* the EPR effect.<sup>30</sup> Once there, the folic acid targeting ligand can facilitate cell uptake process,<sup>31–33</sup> and the subsequent drop in pH during endosomal maturation<sup>45</sup> can very efficiently affect release of the encapsulated triptolide.

**pH-Dependent Drug Release and Inhibition Effects of Nf-Trip in HCC Cells *In Vitro*.** We next investigated the pH-dependent drug release and inhibition effects of Nf-Trip in HCC cells

*in vitro*. Cell cytotoxicity can be driven by intracellular pH-triggered release following folate receptor-mediated endocytosis, thus *in vitro* drug release and efficacy of Nf-Trip were examined. The pH-driven release of triptolide from Nf-Trip is expedited at pH 6 (tumor endosomal pH) compared to pH 7.4 (systemic circulation) (Figure 3a,b). We observed that Nf-Trip more effectively inhibits the viability of FR<sup>+</sup> Bel-7404 cells compared with that of FR<sup>-</sup> MIHA cells (Figure 3c). Additionally, the Nf-Trip showed a stronger inhibition of FR<sup>+</sup> Bel-7404 cell growth at pH 6.0 (Figure 3d) while simultaneously showing decreased cytotoxicity to the normal FR<sup>-</sup> MIHA cells at pH 7.4 (Figure 3e). Furthermore, extracellularly released triptolide has a greatly decreased effect compared to that of Nf-Trip at lower concentrations regardless of cell type or pH as seen *in vitro* (Figure 3d,e). Untargeted Nf-Trip (Nf-Trip-FR<sup>-</sup>) was also selected as a negative control for cytotoxicity studies. This formulation showed a greatly decreased effect compared to Nf-Trip for FR<sup>+</sup> Bel-7404 cells but similar effect of Nf-Trip to FR<sup>-</sup> MIHA cells at both pH 7.4 and 6 (Figure S8 in the Supporting Information). Thus, the major driving force of cytotoxicity appears to come from folate-mediated intracellular release, which is much more pronounced in the FR<sup>+</sup> Bel-7404 cells compared to the FR<sup>-</sup> MIHA cells (Figure 3c–e). Due to the highly cancer-selective nature of the Nf-Trip nanoparticles observed *in vitro* (Figure 3c–e), the pH-dependent intracellular drug release can greatly reduce the toxicity to nontumoral tissues and cells. The cytotoxic effects on liver cancer cells may be associated with influences on cell cycle regulation. The effects of Nf-Trip on FR<sup>+</sup> HCC cell cycle arrest were analyzed by PI staining and flow cytometry. There appears to be a doubling of cells undergoing cell cycle arrest in G2/M phase in FR<sup>+</sup> HCC cells treated with Nf-Trip compared with control (G2/M phase: 25.29% in Nf-Trip vs 11.44% in control) (Figure 3f). The effects of Nf-Trip on apoptosis and DNA damage in FR<sup>+</sup> Bel-7404 and FR<sup>-</sup> MIHA cells at pH 7.4 were also examined using terminal deoxynucleotidyl transferase-mediated nick-end labeling (TUNEL) and DNA damage marker P-H2AX staining by immunofluorescence. The results show both apoptosis and DNA damage are heavily induced in FR<sup>+</sup> HCC cells with Nf-Trip treatment but minimal in FR<sup>-</sup> MIHA cells (Figure 3g,h), indicating the specific targeting and inhibition effect of Nf-Trip on FR<sup>+</sup> HCC cells *in vitro*.

#### Patients' Survival Associated Gene Downregulation by Nf-Trip.

In addition to the toxicity study, we were interested in considering the mechanism of action, particularly on a genetic level. To identify any potential downstream targets, a gene expression profile was generated for Bel-7404 cells treated with Nf-Trip (10 ng/mL triptolide), folate targeted nanoparticles *sans* the triptolide cargo as negative control (Nf-Control) or DMSO solvent control. The top 20 genes where decreased expression was observed (Table 1) were further examined. The microarray data was further validated by real time RT-PCR. The results showed that both CKS2 and AURKA were

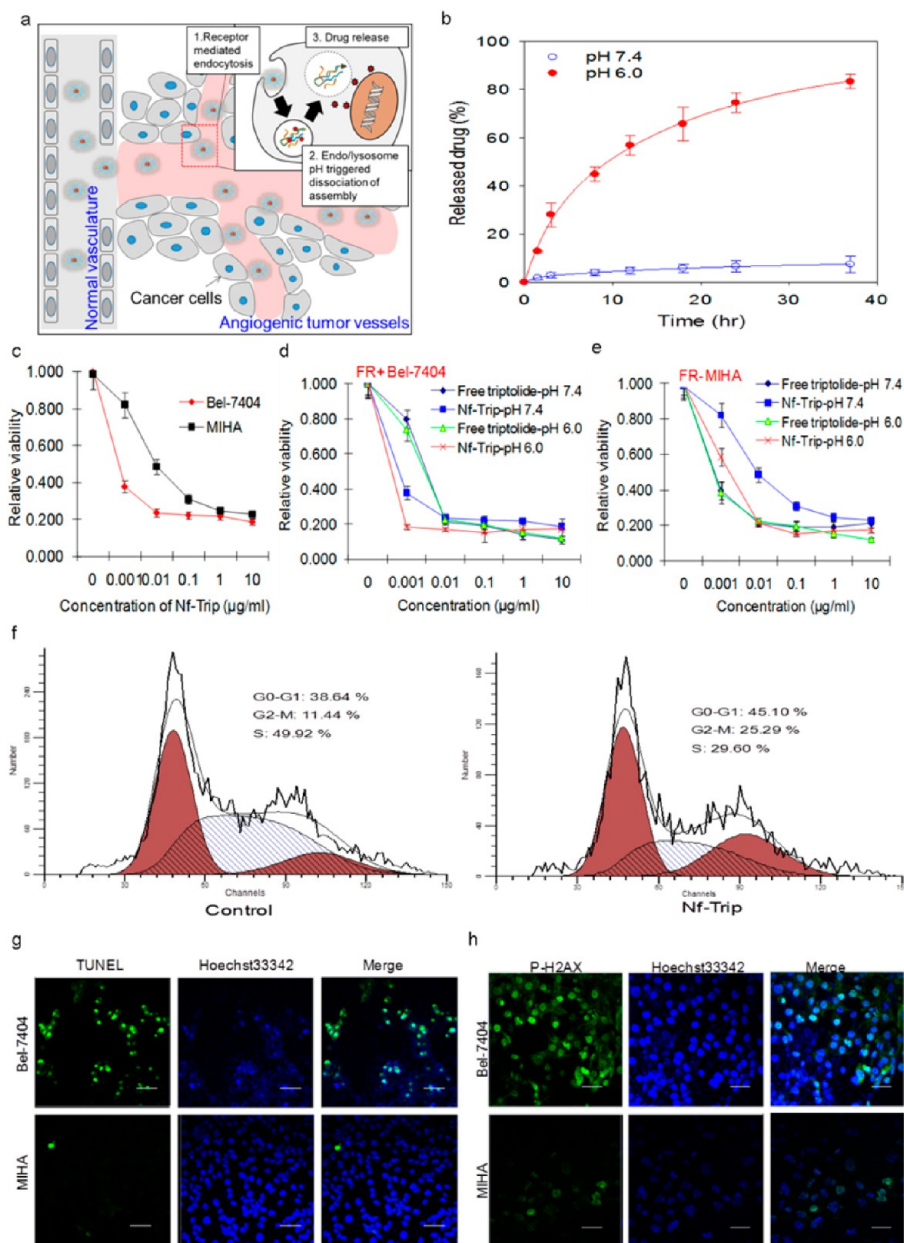


**Figure 3. Targeted drug release and inhibitory effects of Nf-Trip on HCC cells *in vitro*.** (a) Schematic illustration of folate and pH targeted drug release of nanoformulated triptolide (Nf-Trip) in tumor microenvironment. (b) pH-dependent drug release of triptolide from Nf-Trip. (c) Growth inhibitory effects of Nf-Trip on FR<sup>+</sup> Bel-7404 and FR<sup>-</sup> MIHA cells analyzed by MTS. (d and e) Inhibitory effects of Nf-Trip and free triptolide on Bel-7404 and MIHA cells at pH 6.0 and pH 7.4 analyzed by MTS. (f) Effects of Nf-Trip on Bel-7404 cell cycle arrest at G2/M analyzed by flow cytometry. (g) Apoptosis induction by Nf-Trip treatment in Bel-7404 and MIHA cells analyzed by TUNEL. Scale bars, 50  $\mu$ m. (h) Representative images of DNA damage induced by Nf-Trip analyzed by P-H2AX staining. Scale bars, 50  $\mu$ m.

downregulated in HCC cells following the treatment by Nf-Trip (Figure 4a,b). Since preclinical data regarding HCC appears to vary model-to-model,<sup>46–48</sup> it is beneficial to examine these results in the context of a clinical data set that may be more reliable and relevant. Our group has previously established a global gene profile database on HCC tumor tissues and histologically normal liver tissues using Affymetrix Human Genome U133 plus 2.0 Arrays (Affymetrix, Santa Clara, CA).<sup>49–51</sup> This was used to analyze the expression levels of CKS2 and AURKA in patients' HCC tissue samples, and it was found

that both CKS2 and AURKA are significantly upregulated in human HCC samples compared with matched adjacent normal or histologically normal liver tissues (Figure 4c,d). The median expression value of CKS2 and AURKA in all 76 HCC samples studied was chosen as the cutoff point. The Fisher's exact test and Kaplan–Meier analysis showed that high-level expression of CKS2 and AURKA was significantly associated with patients' survival (Figure 4e,f). To further examine if CKS2 and AURKA are involved in the Nf-trip mechanism, we silenced their expression *via* siRNA and examined

**TABLE 1. Top 20 Decreased Expression Genes by Triptolide in HCC Cells**

Transcript Cluster ID	Gene Symbol	Fold Change (Triptolide/Control)
8030002	ZNF114	-25.3734
8077441	BHLHE40	-17.2767
8156290	<b>CKS2</b>	-13.5553
8055688	RND3	-12.9608
7962537	SLC38A2	-12.0721
7904726	TXNIP	-11.3302
7908978	ZC3H11A	-11.2426
8161919	TLE1	-10.1573
8117377	HIST1H1E	-10.0923
8054930	MKI67IP	-9.83051
7934979	ANKRD1	-9.82121
7988838	LEO1	-9.72329
8067167	<b>AURKA</b>	-9.25794
8160297	PLIN2	-9.05077
8087874	WDR82	-9.02924
8164701	SETX	-8.88432
8113073	ARRDC3	-8.389
8050565	PUM2	-8.33998
8041149	WDR43	-8.17517
8077528	SETD5	-8.02955

the response to Nf-trip. We observed that knockdown of both CKS2 and AURKA partially inhibited cell viability and significantly decreased the cellular response to triptolide (Figure S9 in the Supporting Information), suggesting that both CKS2 and AURKA are major contributors to triptolide's mechanism of action. These results further indicate that our Nf-Trip can be important therapeutic target for HCC because CKS2 and AURKA indeed play important roles in hepatocarcinogenesis.

**In Vitro and *in Vivo* Distribution of Nf-Trip in FR<sup>+</sup> HCC Cells and Orthotopic Mice Models.** Next, the *in vitro* cellular uptake efficiency of the Nf-Trip was examined for folate receptor overexpression by comparing FR<sup>+</sup> HCC cell line (Bel-7404, Figure S10 in the Supporting Information) with FR<sup>-</sup> normal hepatocytes (MIHA, Figure S10 in the Supporting Information). When it was incubated with FR<sup>-</sup> MIHA cells, Nf-Trip showed very little cellular uptake, whereas uptake into FR<sup>+</sup> Bel-7404 was highly efficient, thus demonstrating excellent cell-specific efficacy as shown by live cell imaging with differential interference contrast (DIC) microscopy (Figure 5a). Next, confocal laser scanning microscopy (CLSM) was used to further examine Nf-Trip uptake into FR<sup>+</sup> HCC cells, which showed diffuse intracellular fluorescence with only a minimal amount of intracellular fluorescence within FR<sup>-</sup> MIHA cells (Figure 5b). However, when an excess amount of folic acid (FA) was added to compete with Nf-Trip-FR<sup>+</sup>, the cellular uptake of the particles greatly decreased resulting in a minimal amount of intracellular fluorescence within FR<sup>+</sup> HCC cells (Figure S11 in the Supporting Information). This suggests the folic acid, with specific binding to folate receptors on the HCC cells, is effectively driving the endocytosis of Nf-Trip-FR<sup>+</sup>. This is further supported by the lack of endocytosis of Nf-Trip-FR<sup>-</sup>, even in the absence of competitive folate ligands (Figure S10 in the Supporting Information).

To analyze tumor targeting *in vivo*, we used a custom HCC orthotopic xenograft model developed from luciferase expressing FR<sup>+</sup> HCCs. The FR<sup>+</sup> Bel-7404 cells transfected with the luciferase vector were subcutaneously implanted and grown in nude mice. These ectopic tumors were then excised, and small tumoroids were surgically implanted orthotopically into the liver of new mice (Figure S12 in the Supporting Information). Once the orthotopic xenograft tumors were established, treatments began with Nf-Trip (with and without surface folate ligand, 1 mg equiv/kg) administered intravenously by tail vein injection twice per week. The whole body distribution of Nf-Trip by RITC was imaged using the Xenogen IVIS Lumina system following tail vein injection. After 20 h, a large accumulation of the Nf-Trip-FR<sup>+</sup> was found in the liver tumor tissue using the Xenogen system, which showed colocalization with the luciferase signal from the implanted tumor cells (Figure 5c). Nf-Trip-FR<sup>-</sup> also showed some tumor accumulation due to local EPR effect of nanoparticles in the inflamed tumor tissue,<sup>30</sup> but the nanoparticle signal of Nf-Trip-FR<sup>-</sup> is much weaker than that of Nf-Trip-FR<sup>+</sup> (Figure S13 in the Supporting Information). The increased uptake of Nf-Trip-FR<sup>+</sup> compared to Nf-Trip-FR<sup>-</sup> demonstrated the folate targeting.

**Nf-Trip Reduces Tumor Burden and Improves Survival without Toxicity in Orthotopic Mouse Models.** To examine the efficacy of our nanoformulated triptolide, we used an orthotopic HCC model that expresses luciferase (Figure 6). Since the tumor cells grow in the liver, this is a better model of a natural tumor; however, it is more difficult to examine the changes in size for deep tissue tumors. The luciferase in these tumors allows imaging *via* the Xenogen IVIS Lumina system providing a great advancement in terms of clinical relevance. Treatments began once the orthotopic xenograft tumors were established. The test

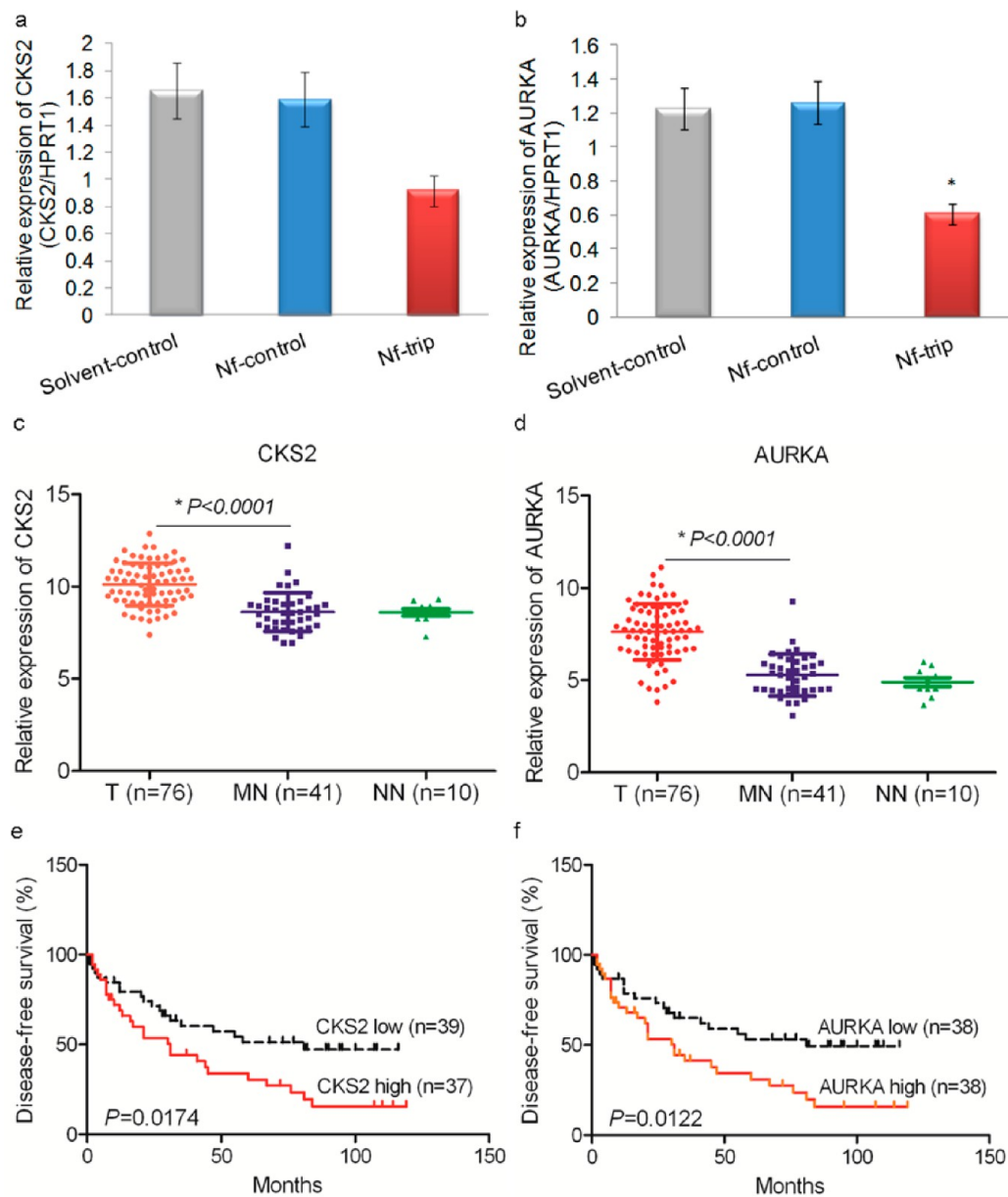


**Figure 4.** Two biomarkers associated with clinical patients' survival in HCC, CKS2 and AURKA, are potential downstream targets of Nf-Trip. (a and b) The downregulation of cell cycle and apoptosis related cyclin kinase subunit-2 (CKS2) and aurora A kinase (AURKA) by Nf-Trip treatment was validated by RT-qPCR. (c and d) The expression of CKS2 and AURKA was significantly increased in a group of HCC patients' tissue samples compared to matched adjacent nontumor tissues by RT-qPCR analysis (T, tumoral liver tissue; MN, matched adjacent nontumor liver tissue; NN, histologically normal liver tissue). (e and f) Fisher's exact test and Kaplan-Meier analysis showed the high expression of CKS2 and AURKA is correlated with poor survival prognoses in HCC patients. The median value of CKS2 and AURKA expression in all 76 HCC samples studied was chosen as the cutoff point.

formulations included Nf-Trip (Nf-Trip-FR<sup>+</sup>, 1 mg equiv/kg), untargeted Nf-Trip (Nf-Trip-FR<sup>-</sup>, 1 mg equiv/kg), free triptolide (1 mg/kg) and blank, folate targeted nanoparticles *sans* the triptolide cargo as negative control (Nf-Control). All treatments were administered intravenously by tail vein injection twice per week. The therapeutic efficacy was determined by measuring tumor size as estimated from the bioluminescence signal following luciferin administration. Among all treatment groups, the Nf-Trip-FR<sup>+</sup> showed the greatest efficacy. This was confirmed by both the luciferase signal and physical examination of the excised liver organs (Figure 6a–c) following

the study. The enhanced efficacy of Nf-Trip-FR<sup>+</sup> compared to free triptolide is likely a result of passive accumulation of nanoparticles in the inflamed tumor tissue.<sup>30</sup> However, subcellular CLSM of the tumor tissue confirmed the increased uptake of Nf-Trip-FR<sup>+</sup> and Nf-Control by the vicinal cells in tumor region compared to Nf-Trip-FR<sup>-</sup> due to folate targeting. Immunofluorescence staining of the tumor tissues to differentiate cancer cells from kupffer cells further confirmed that RITC-labeled Nf-Trip is internalized preferentially by the tumor cells (Figure 6e). Furthermore, the immunohistochemical staining of Kupffer cells marker CD68 in the tumor tissues shows most of

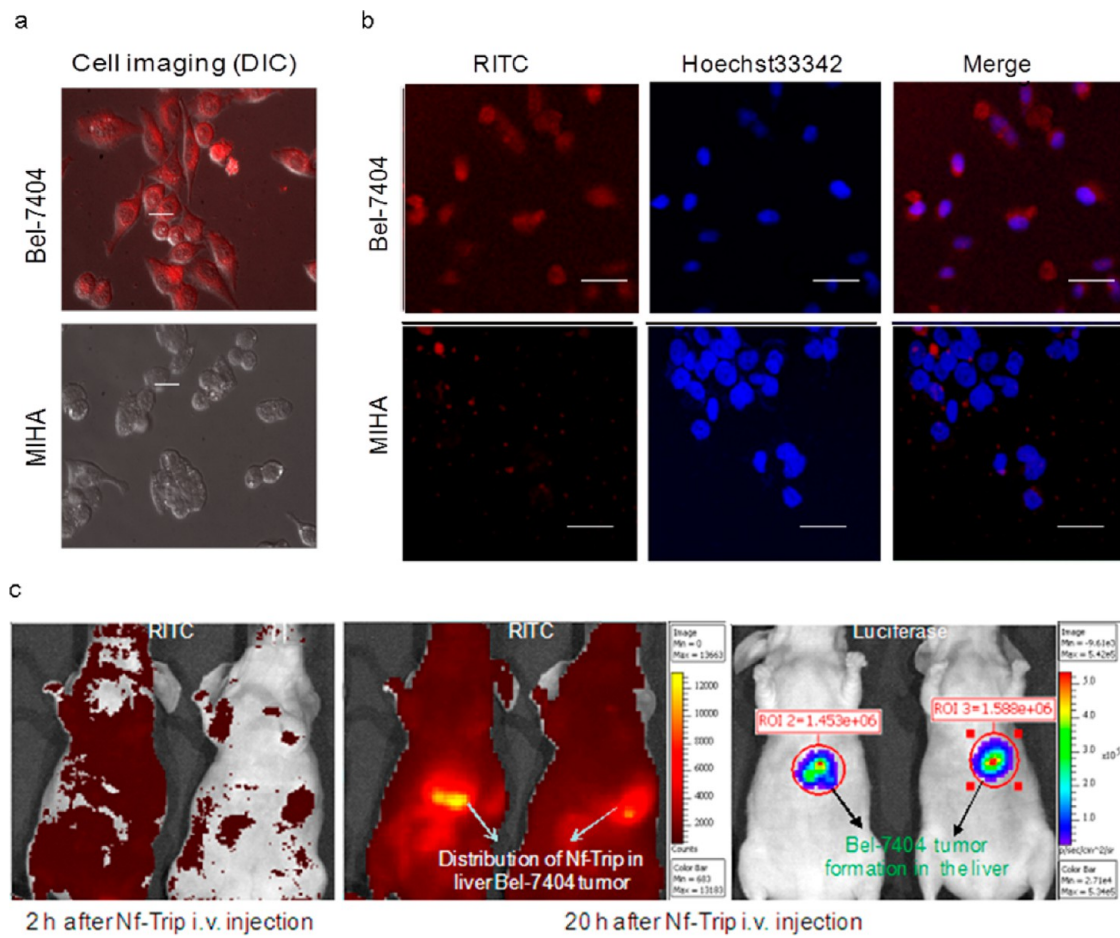


**Figure 5.** Cell uptake and *in vivo* biodistribution of Nf-Trip in FR<sup>+</sup> HCC cells and orthotopic mouse models. (a) Representative cellular uptake images of Nf-Trip (10 ng/mL) in FR<sup>+</sup> Bel-7404 liver cancer cells and FR<sup>-</sup> hepatic parenchymal cells (MIHA) using the Nikon live cell imaging fluorescence microscopy system with DIC. Scale bars, 20  $\mu$ m. (b) Representative cellular uptake images of Nf-Trip in FR<sup>+</sup> Bel-7404 and FR<sup>-</sup> MIHA cells using CLSM. Scale bars, 50  $\mu$ m. (c) Representative *in vivo* imaging of mice bearing luciferase expressing orthotopic HCC tumors derived from FR<sup>+</sup> Bel-7404 cells following intravenous injection of Nf-Trip (containing RITC) using the Xenogen IVIS Lumina system.

the Nf-Trip was taken up by HCC cancer cells, not Kupffer cells (Figure 6f), further demonstrating excellent selectivity.

In terms of toxicity, the Nf-Control group and Nf-Trip (with or without folate receptor) treated mice showed stable weight levels, whereas free triptolide led to substantial weight loss (Figure 6d). The liver and renal toxicity of the formulation has been further investigated through typical clinical chemistry (ALT, AST, BUN). The results showed both the empty Nf-Control and Nf-Trip formulation (with or without folate receptor) have minor associated toxicities, while free triptolide showed greatly increased toxicity (Figure S14 in the Supporting Information). Histopathological examination also demonstrated the increased biocompatibility of NF-Trip compared to free triptolide (Figure S14 in the Supporting Information). These results demonstrated that the high toxicity of triptolide was mitigated by using a targeted formulation. In terms of survival, Nf-Trip treated mice showed ~80% survival after 3 months with ~50% survival for free triptolide and ~30% survival for

the untreated control (Figure S15 in the Supporting Information).

To further determine the efficacy at the cellular level, the tumors were harvested and histochemically examined following the pharmacodynamic study. Hematoxylin and eosin staining (H&E) and immunohistochemical (IHC) staining of tumor tissues for CKS2 and AURKA showed that the Nf-Trip-treated tumor was much more necrotic compared to the free triptolide-treated tumors, and no necrosis was observed in the nontreated DMSO control group (Figure S16 in the Supporting Information). Consistent with the *in vitro* results, TUNEL staining also confirmed there is a greater population of cells undergoing apoptosis in the Nf-Trip-treated tumor tissues compared to free triptolide-treated tumors and the nontreated DMSO control group (Figure S16 in the Supporting Information). Lastly, IHC staining further showed that the expression of CKS2 and AURKA was significantly decreased in the Nf-Trip-treated tumor tissues compared with free triptolide- or the nontreated tumor tissues (Figure S17 in the Supporting Information).

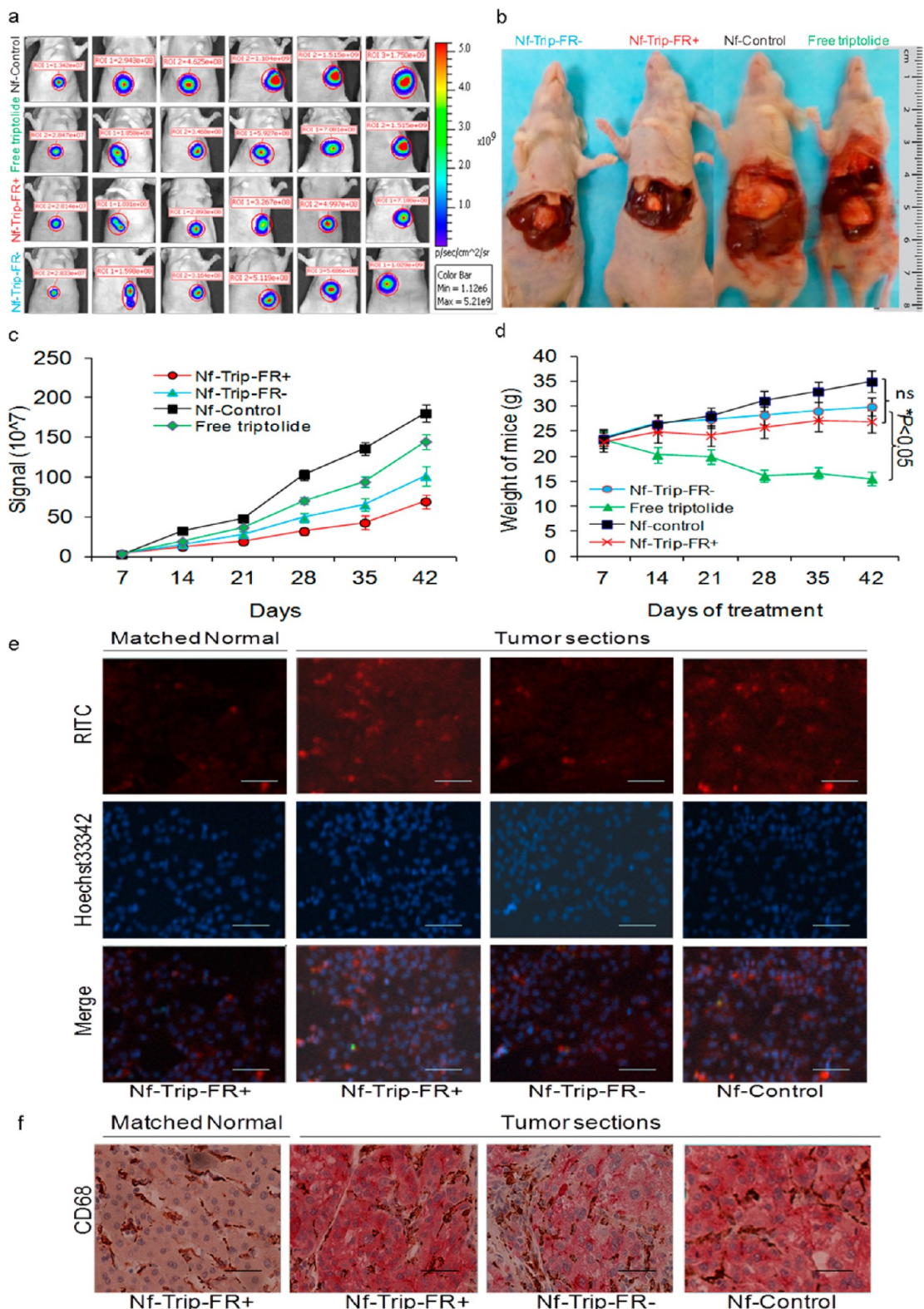


**Figure 6.** Nf-Trip reduces the tumor burden while mitigating the toxicity in orthotopic mouse models. (a) Representative weekly images of orthotopic tumor xenografts during treatment. (b) Representative tumor-bearing livers in mice at the therapeutic end point of different treatments. (c) Quantitative analysis of weekly bioluminescence signals of all mice for the four treatment groups. (d) Average weekly mouse body weight for the four treatment groups. (e) CLSM shows nanoparticle uptake by tumor cells following intravenous injection. Scale bars, 50  $\mu$ m. (f) Immunohistochemical staining of CD68 (Kupffer cells) in the tumor tissues shows most of the nanoparticles were preferentially taken up by the cancer cells. Scale bars, 20  $\mu$ m.

## CONCLUSIONS

Triptolide has gained a great deal of interest lately in cancer therapy due to its effectiveness in a variety of cancer cells.<sup>10–16</sup> However, as with most preclinical leads, positive *in vitro* data does not directly correlate with positive *in vivo* data due to poor solubility and minimal accumulation at the target site, leading to significantly increased systemic toxicity. By developing Nf-Trip, we were able to solubilize the drug for intravenous administration and take advantage of the size-dependent accumulation of nanoparticles in inflamed tumoral tissues. By using rationally designed synthetic polymers in the Nf-Trip nanoparticles, we were successfully able to make them responsive to the acidic microenvironment of the tumor, thereby increasing site-specific drug release as well as affecting tumor

cell-specific uptake for increased efficacy and decreased toxicity. Ordinarily, HCC is very aggressive with very poor prognosis, which we have correlated with elevated expression levels of CKS2 and AURKA. These two proteins appear to be downregulated, which may be one reason for the drug's potency in HCC therapy. Coupling this with directed drug delivery in a specific subset of the affected population, in this case FR<sup>+</sup> tumors, led to greatly increased progression-free survival in mice with fewer observable side effects. As our data suggests, highly potent drugs like triptolide come with too high a risk of toxicity, so it is relevant to consider that rationally designed nanoformulation can help offset the toxicity leading to improved outcomes and hopefully facilitate their translation into clinical studies.

## METHODS

**Materials.** All reagents and solvents were obtained commercially and used without further purification. Pluronic F127,  $\beta$ -benzyl-L-aspartate (BLA), bis(trichloromethyl)carbonate (triphosgene), 1-(3-aminopropyl)imidazole (API), octadecylamine, folate, thiazolyl blue tetrazolium bromide, dicyclohexylcarbodiimide (DCC), 4-(dimethylamino)pyridine (DMAP), sephadex LH-20, *N,N*-dimethylformamide (DMF), tetrahydrofuran (THF), dichloromethane and (CH<sub>2</sub>Cl<sub>2</sub>), and dimethyl sulfoxide (DMSO) were purchased from Sigma-Aldrich Co. (St. Louis, MO). BLA-NCA was synthesized by the Fuchs-Farthing method using triphosgene.<sup>52,53</sup> Dimethyl sulfoxide-*d*<sub>6</sub> (DMSO-*d*<sub>6</sub>, 99% D) was purchased from Cambridge Isotope Laboratories, Inc. (Andover, MA). The dialysis membranes were obtained from Spectrum Laboratories, Inc. (Rancho Dominguez, CA). Roswell Park Memorial Institute (RPMI-1640) medium, Dulbecco's Modified Eagle Medium (DMEM), fetal bovine serum (FBS), antibiotics (penicillin/streptomycin), and Dulbecco's phosphate buffered saline (DPBS) were obtained from Gibco BRL (Invitrogen Corp., Carlsbad, CA). Doxorubicin, daunorubicin, and sorafenib were products from Bayer HealthCare Pharmaceuticals, Inc. Triptolide (CAS No. 38748-32-2, 99% by HPLC) was obtained from Chengdu Biopurity Phytochemicals, Ltd. (China).

**Synthesis of Folate (FA)–Pluronic F127 (PF127) conjugates.** Pluronic F127 powder (100 mg) was dissolved in anhydrous DMSO. Folic acid (5 mg, 1.5 equiv) was dissolved in DMSO (10 mL), followed by the addition of 1.5 mol equiv of DCC and DMAP. Pluronic F127 was dissolved in DMSO with vigorous stirring and subsequently mixed slowly with the activated folic acid. The reaction mixture was then gently stirred for 24 h at room temperature. The reaction mixture was dialyzed (MWCO: 1000 Da) for 2 days against distilled water to remove unconjugated folic acid and DMSO. The final solution was flash-frozen and lyophilized. The crude folic acid–Pluronic F127 conjugates were purified using Sephadex LH-20 (Sigma-Aldrich, Co.).<sup>54</sup>

<sup>1</sup>H NMR (500 MHz, DMSO-*d*<sub>6</sub>) for folic acid–pluronic F127 conjugate (Figure S1):  $\delta$  = 8.6 ppm (1H, d, –N=CH<sub>2</sub>CH<sub>2</sub>– of folic acid), 7.6 ppm (t, 1H, –CH=CH– of folic acid), 6.6 ppm (t, 1H, –CH=CH– of folic acid), 3.4–3.6 ppm (m, 848H, –CH<sub>2</sub>CH<sub>2</sub>O– of pluronic F127), and 1.0 ppm (d, 210H, –CH<sub>2</sub>CH<sub>2</sub>–(CH<sub>3</sub>)O– of pluronic F127).

**Synthesis of Octadecylamine–p(API-Asp)<sub>10</sub>.**  $\beta$ -Benzyl-L-aspartate *N*-carboxy anhydride (BLA-NCA) (3 g, 12 mmol) was polymerized in a mixture of DMF (20 mL) and CH<sub>2</sub>Cl<sub>2</sub> (50 mL) at 40 °C by initiation from the terminal primary amino group of octadecylamine (MW = 269.51 g/mol, 0.3 g, 1.2 mmol). The reaction mixture was stirred for 2 days. The reaction solution was rotovapped under high vacuum to remove the CH<sub>2</sub>Cl<sub>2</sub>. The polymer was precipitated by the slow addition of 0.1 N HCl

(20 mL) followed by centrifugation (3000 rpm) for 5 min. The supernatants were discarded, and the residue was lyophilized to remove remaining water. pH-sensitive octadecylamine–p(API-Asp)<sub>10</sub> was synthesized via aminolysis of the octadecylamine–PBLA with 1-(3-aminopropyl)imidazole (API). Octadecylamine–p(API-Asp)<sub>10</sub> (0.2, 74.8  $\mu$ mol) was dissolved in DMSO (5 mL), followed by the reaction with API (1 g, 7.9 mmol) under nitrogen at 25 °C, and stirred for 12 h. The reaction mixture was added dropwise into a cooled aqueous solution of 0.1 N HCl (20 mL) and dialyzed against a 0.01 N HCl solution three times (Spectra/Por; MWCO: 1000 Da). The final solution was lyophilized to obtain octadecylamine–p(API-Asp)<sub>10</sub> as a white solid.

<sup>1</sup>H NMR (500 MHz, DMSO-*d*<sub>6</sub>) for octadecylamine–p(API-Asp)<sub>10</sub> (Figure S2 in Supporting Information):  $\delta$  = 7.8 ppm (1H, s, –NCH=N– of imidazole ring), 7.7 ppm (1H, s, –NCH=CH– of imidazole ring), 7.3 ppm (1H, s, –CH=CH–N– of imidazole ring), 4.5 ppm (1H, m, –NHCHC=O–), 4.0 ppm (2H, s, =NCH<sub>2</sub>CH<sub>2</sub>), 3.0 ppm (2H, s, –NHCH<sub>2</sub>CH<sub>2</sub>–), 2.6 ppm (2H, m, –CH<sub>2</sub>C=ONH–), 1.8 ppm (2H, s, –CH<sub>2</sub>CH<sub>2</sub>CH<sub>2</sub>–), 1.2 ppm (17H, s, –CH<sub>2</sub>– of octadecylamine), and 0.8 ppm (3H, t, CH<sub>3</sub>– of octadecylamine).

**Synthesis of Fluorescence (RITC) Labeled Octadecylamine–p(API-Asp)<sub>10</sub>.** Octadecylamine–p(API-Asp)<sub>10</sub> (100 mg) in DMSO (20 mL) was reacted with RITC (30 mg) for 12 h at room temperature in the dark. The reaction mixture was dialyzed (MWCO: 1000 Da) for 2 days against distilled water to remove unlabeled RITC and DMSO.

**Preparation of Nf-Trip.** The octadecylamine–p(API-Asp)<sub>10</sub> (20 mg), FA–F127 (20 mg), and drug (4 mg) were dissolved in methanol (6 mL) and dried into a film on the wall of 25 mL round-bottom flask at 60 °C under reduced pressure. Then, 5 mL of PBS (pH 7.4) was subsequently added into the flask to hydrate the formed film. After ultrasonication for 5 min with a probe sonicator (Sonics Vibra cell, Sonics & Material, Inc., New Town, CT), the solution was stirred continuously at 60 °C for 6 h. To remove unloaded drug, the sample was dialyzed against PBS (pH 7.4) for 12 h. Untargeted Nf-Trip (Nf-Trip-FR<sup>–</sup>) was prepared by using F127 instead of FA–F127 following the same procedure.

**Cell Lines and Cell Culture.** Human liver cancer cells (Bel-7404 and HCCLM3) or immortalized normal hepatocyte cells (MIHA) were cultured in DMEM containing 10% fetal bovine serum (FBS) and 1% penicillin–streptomycin. The cells were maintained at 37 °C in the presence of 5% CO<sub>2</sub>.

**In Vitro Cellular Uptake Study.** After reaching confluence, cells were detached, counted, and seeded in the 8-well cover-glass chamber (LAB-TEK, Nalge Nunc, IL) overnight. Then, the medium was replaced by Nf-Trip spiked medium at different concentrations and incubated for different lengths of time. The cellular uptake of Nf-Trip was observed using a Nikon live cell imaging system (Nikon). The cellular uptake behavior and intracellular distribution of the Nf-Trip were also analyzed using

confocal laser scanning microscopy (CLSM) (Carl Zeiss). The cells treated with Nf-Trip were washed twice with prewarmed 1× PBS and fixed with 4% paraformaldehyde for 15 min. The cells were then washed twice with PBS, and the nuclei were counterstained with Hoechst 33342 and imaged by CLSM. Data were processed with Adobe Photoshop 7.0 software for analysis.

**In Vitro Cytotoxicity.** The liver cancer cells or immortalized normal hepatocyte (MIHA) cells were seeded into 96-well plates at a density of  $5 \times 10^3$  cells/well (100  $\mu$ L). The medium was replaced by Nf-Trip spiked medium at various concentrations for different time points. For the MTS assay, the CellTiter 96 AQueous One Solution Cell Proliferation Assay kit (Promega, Madison, WI) was used following the manufacturer's instructions. Briefly, at 2 h before each of the desired time point treatments, 20  $\mu$ L of the MTS reagent was added into each well and cells were incubated at 37 °C for another 2 h. The absorbance was detected at 490 nm using a Wallac Victor 1420 Multilabel plate reader. All experiments were repeated in triplicate.

**Apoptosis Analysis (TUNEL).** For labeling nuclei of apoptotic cells, HCC cells treated with Nf-Trip or controls were plated on glass coverslips in 24-well plates and fixed in 4% paraformaldehyde 24 h post-Nf-Trip treatment. For apoptosis detection in tissue sections, the slides were washed twice in xylene to remove paraffin and rehydrated by washing slides in decreasing concentrations of ethanol. TUNEL staining was done using the DeadEnd fluorometric TUNEL system (Promega) according to the manufacturer's protocol. The number of TUNEL-positive cells was divided by the number of Hoechst 33342-stained cells to yield the percent apoptotic nuclei. Two 40 $\times$  objective fields containing  $\sim 100$  cells each were counted per coverslip, with three coverslips analyzed per condition.

**DNA Damage Analysis.** The HCC cells were seeded in the BD Falcon 8-well CultureSlide and treated with Nf-Trip or controls for 24 h. The treated cells were fixed and incubated with primary antibodies against p-H2AX and then incubated with secondary antibody Alexa Fluor 488 goat anti-rabbit IgG (Invitrogen). Slides were counterstained with Hoechst 33342 and imaged using confocal laser scanning microscopy (CLSM).

**Microarray and Real-Time Quantitative RT-PCR (qRT-PCR) Analysis.** Total RNA from the tissue samples, Bel-7404 cells treated with Nf-Trip, or solvent control was extracted using TRIzol reagent (Invitrogen). The quality and quantity of isolated total RNA were assessed using the Agilent 2100 Bioanalyzer and NanoDrop ND-1000 Spectrophotometer (Agilent, Santa Clara, CA). Microarray analysis was performed as we described in our previous report<sup>46</sup> using the GeneChip Human Gene ST Arrays (Affymetrix) according to the manufacturers' instructions. For mRNA detection by qRT-PCR, the total RNA was reversely transcribed using SuperScript III First-Strand Synthesis System for RT-PCR (Invitrogen, CA). qPCR was performed using SsoFast EvaGreen Supermix (Bio-Rad) with hypoxanthine phosphoribosyltransferase 1 (HPRT1) as an internal control, and concentration differences were calculated via relative quantification ( $2^{-\Delta C_t}$ ). The survival curves were created using the Kaplan-Meier method and statistically compared using a log-rank test.<sup>46</sup>

**Flow Cytometry.** The cell cycle was analyzed by flow cytometry (FACSCanto II, BD Biosciences) using PI staining (BD Biosciences) according to the standard protocol. Briefly, 1 day before the treatment, equal numbers of cells ( $2.0 \times 10^5$ ) were seeded into 6-well tissue culture plates. The cells were then treated with Nf-Trip (0.01  $\mu$ g/mL) or solvent control. After 24 h treatment, the cells were fixed in ice-cold 70% ethanol and stained using the Coulter DNA-Prep Reagents kit (Beckman Coulter, Fullerton, CA). Cellular DNA content of  $5 \times 10^5$  cells from each sample was then determined by flow cytometry (FACSCanto II, BD Biosciences). Cell cycle phase distribution was analyzed with FlowJo software using data obtained from two separate experiments in which each treatment was performed in triplicate.

**Immunohistochemistry (IHC).** The paraffin-embedded tissue samples from consenting patients were cut in 5- $\mu$ m sections and placed on polylysine coated slides, deparaffinized in xylene, and rehydrated using a series of graded alcohols. Antigen retrieval was performed by heat mediation in citrate buffer (pH 6) (Dako). Samples were blocked with 10% goat serum

before incubating with primary antibody. The samples were incubated overnight using a primary antibody, anti-CKS2 and AURKA (1:100) (Abcam), or an isotype-matched IgG as a negative control in a humidified container at 4 °C. Immunohistochemical staining was performed with the Dako Envision Plus System (Dako, Carpinteria, CA) according to the manufacturer's instructions. The intensity of staining was evaluated on the scale of 0 to 4 according to the percentage of positive tumors.

**Orthotopic HCC Models.** All experiments using mice were approved by the SingHealth Institutional Animal Care and Use Committee (IACUC). Bel-7404 luciferase expression cells were first subcutaneous injected into 5- to 6-weeks old athymic mice (BioLASCO Taiwan Co., Ltd.) to generate tumors. Then, the mice were anesthetized with Hypnorm/Midazolam and the tumors excised and cut into pieces. Similar sized tumoroids were transplanted into the liver of new mice to establish the orthotopic xenograft liver tumor models. One week after the surgery, the mice were imaged and grouped based on equivalent signal intensity. The mice were then treated with Nf-Trip- $FR^+$ , Nf-Trip- $FR^-$ , empty Nf-control, free triptolide or vehicle via semiweekly intravenous injections for 7 weeks. Tumor growth was measured weekly by bioluminescence imaging using the Xenogen IVIS Lumina system (Xenogen Corporation, Hopkinton, MA). Briefly, following anesthesia with 2% isoflurane, mice were IP injected with d-Luciferin (150 mg/kg; Caliper Life Sciences, Inc., Hopkinton, MA) and subjected to 1 s to 1 min scans to assess the bioluminescent signal.

**Survival and Statistical Analysis.** The experimental data are presented as the mean  $\pm$  standard deviation (SD). All statistical analyses were performed using ANOVA or a two-tailed Student's *t* test (GraphPad Prism 5). The survival curves were created using the Kaplan-Meier method and statistically compared using a log-rank test. Differences were considered statistically significant when the *P*-values were less than 0.05.

**Conflict of Interest:** The authors declare no competing financial interest.

**Acknowledgment.** T.H. acknowledges financial support by the Research Center Program of Institute for Basic Science (IBS) in Korea; K.M.H. and H.P.X. acknowledge financial support by the SingHealth Foundation, National Medical Research Council, Biomedical Research Council of Singapore and The Singapore Millennium Foundation. We thank Dr. Tony Lim (Pathologist, Singapore General Hospital) for helping on immunohistochemical staining and Dr. James Zhao (SingHealth Advanced Bioimaging Core, Singapore Health Services) for helping on confocal laser scanning microscopy (CLSM).

**Supporting Information Available:** Synthetic scheme and  $^1$ H NMR spectra of folate-pluronic F127 conjugates, octadecylamine-p(API-Asp)<sub>10</sub>, cytotoxicity comparison of triptolide with conventional agent for HCC, the triptolide calibration curve of HPLC, flow cytometry for HCC cells treated with triptolide, RT-qPCR analysis of relative expression level of folate receptor (FOLR1) on various HCC cells, and the procedure for luc-expressing, orthotopic xenograft model development. This material is available free of charge via the Internet at <http://pubs.acs.org>.

## REFERENCES AND NOTES

1. Maluccio, M.; Covey, A. Recent Progress in Understanding, Diagnosing, and Treating Hepatocellular Carcinoma. *CA Cancer J. Clin.* **2012**, *62*, 394–399.
2. Avila, M. A.; Berasain, C.; Sangro, B.; Prieto, J. New Therapies for Hepatocellular Carcinoma. *Oncogene* **2006**, *25*, 3866–3884.
3. Abdel-Rahman, O.; Fouad, M. Sorafenib-Based Combination as a First Line Treatment for Advanced Hepatocellular Carcinoma: A Systematic Review of the Literature. *Crit. Rev. Oncol./Hematol.* **2014**, *91*, 1–8.
4. Villanueva, A. Rethinking Future Development of Molecular Therapies in Hepatocellular Carcinoma: A Bottom-Up Approach. *J. Hepatol.* **2013**, *59*, 392–395.
5. Llovet, J. M.; Ricci, S.; Mazzaferro, V.; Hilgard, P.; Gane, E.; Blanc, J.-F.; de Oliveira, A. C.; Santoro, A.; Raoul, J.-L.; Forner,

A. Sorafenib in Advanced Hepatocellular Carcinoma. *N. Engl. J. Med.* **2008**, *359*, 378–390.

- Cheng, A.-L.; Kang, Y.-K.; Chen, Z.; Tsao, C.-J.; Qin, S.; Kim, J. S.; Luo, R.; Feng, J.; Ye, S.; Yang, T.-S. Efficacy and Safety of Sorafenib in Patients in the Asia-Pacific Region with Advanced Hepatocellular Carcinoma: A Phase III Randomised, Double-blind, Placebo-controlled Trial. *Lancet Oncol.* **2009**, *10*, 25–34.
- Phillips, P. A.; Dudeja, V.; McCarroll, J. A.; Borja-Cacho, D.; Dawra, R. K.; Grizzle, W. E.; Vickers, S. M.; Saluja, A. K. Triptolide Induces Pancreatic Cancer Cell Death via Inhibition of Heat Shock Protein 70. *Cancer Res.* **2007**, *67*, 9407–9416.
- Mujumdar, N.; Mackenzie, T. N.; Dudeja, V.; Chugh, R.; Antonoff, M. B.; Borja-Cacho, D.; Sangwan, V.; Dawra, R.; Vickers, S. M.; Saluja, A. K. Triptolide Induces Cell Death in Pancreatic Cancer Cells by Apoptotic and Autophagic Pathways. *Gastroenterology* **2010**, *139*, 598–608.
- Antonoff, M. B.; Chugh, R.; Borja-Cacho, D.; Dudeja, V.; Clawson, K. A.; Skube, S. J.; Sorenson, B. S.; Saltzman, D. A.; Vickers, S. M.; Saluja, A. K. Triptolide Therapy for Neuroblastoma Decreases Cell Viability *in Vitro* and Inhibits Tumour Growth *in Vivo*. *Surgery* **2009**, *146*, 282–290.
- Tengchaisri, T.; Chawengkirkitkul, R.; Rachaphaew, N.; Reutrakul, V.; Sangsuwan, R.; Sirisinha, S. Antitumour Activity of Triptolide against Cholangiocarcinoma Growth *in Vitro* and in Hamsters. *Cancer Lett.* **1998**, *133*, 169–175.
- Zhou, Z.-L.; Yang, Y.-X.; Ding, J.; Li, Y.-C.; Miao, Z.-H. Triptolide: Structural Modifications, Structure–Activity Relationships, Bioactivities, Clinical Development and Mechanisms. *Nat. Prod. Rep.* **2012**, *29*, 457–475.
- Chugh, R.; Sangwan, V.; Patil, S. P.; Dudeja, V.; Dawra, R. K.; Banerjee, S.; Schumacher, R. J.; Blazar, B. R.; Georg, G. I.; Vickers, S. M. A Preclinical Evaluation of Minnelide as a Therapeutic Agent against Pancreatic Cancer. *Sci. Transl. Med.* **2012**, *156*, 156ra139.
- Mura, S.; Nicolas, J.; Couvreur, P. Stimuli-Responsive Nanocarriers for Drug Delivery. *Nat. Mater.* **2013**, *12*, 991–1003.
- Murakami, M.; Cabral, H.; Matsumoto, Y.; Wu, S.; Kano, M. R.; Yamori, T.; Nishiyama, N.; Kataoka, K. Improving Drug Potency and Efficacy by Nanocarrier-Mediated Subcellular Targeting. *Sci. Transl. Med.* **2011**, *3*, 64ra2.
- Cheng, Z.; Al Zaki, A.; Hui, J. Z.; Muzykantov, V. R.; Tsourkas, A. Multifunctional Nanoparticles: Cost versus Benefit of Adding Targeting and Imaging Capabilities. *Science* **2012**, *338*, 903–910.
- Zamboni, W. C.; Torchilin, V.; Patri, A. K.; Hrkach, J.; Stern, S.; Lee, R.; Nel, A.; Panaro, N. J.; Grodzinski, P. Best Practices in Cancer Nanotechnology: Perspective from NCI Nanotechnology Alliance. *Clin. Cancer Res.* **2012**, *18*, 3229–3241.
- Perrault, S. D.; Chan, W. C. W. *In Vivo* Assembly of Nanoparticle Components to Improve Targeted Cancer Imaging. *Proc. Natl. Acad. Sci. U.S.A.* **2010**, *107*, 11194–11199.
- Kircher, M. F.; de la Zerda, A.; Jokerst, J. V.; Zavaleta, C. L.; Kempen, P. J.; Mittra, E.; Pitter, K.; Huang, R.; Campos, C.; Habte, F.; et al. A Brain Tumour Molecular Imaging Strategy Using a New Triple-Modality MRI-Photoacoustic-Raman Nanoparticle. *Nat. Med.* **2012**, *18*, 829–834.
- Zrazhevskiy, P.; Sena, M.; Gao, X. Designing Multifunctional Quantum Dots for Bioimaging, Detection, and Drug Delivery. *Chem. Soc. Rev.* **2010**, *39*, 4326–4354.
- Park, J.; Wrzesinski, S. H.; Stern, E.; Loo, M.; Criscione, J.; Ragheb, R.; Jay, S. M.; Demento, S. L.; Agawu, A.; Limon, P. L.; et al. Combination Delivery of TGF- $\beta$  Inhibitor and IL-2 by Nanoscale Liposomal Polymeric Gels Enhances Tumour Immunotherapy. *Nat. Mater.* **2012**, *11*, 895–905.
- Cabral, H.; Matsumoto, Y.; Mizuno, K.; Chen, Q.; Murakami, M.; Kimura, M.; Terada, Y.; Kano, M. R.; Miyazono, K.; Uesaka, M.; et al. Accumulation of Sub-100 nm Polymeric Micelles in Poorly Permeable Tumours Depends on Size. *Nat. Nanotechnol.* **2011**, *6*, 815–823.
- Omid, C. F.; Langer, R. Impact of Nanotechnology on Drug Delivery. *ACS Nano* **2009**, *3*, 16–20.
- Idris, N. M.; Gnanasammandhan, M. K.; Zhang, J.; C Ho, P.; Mahendran, R.; Zhang, Y. *In vivo* Photodynamic Therapy Using Upconversion Nanoparticles as Remote-Controlled Nanotransducers. *Nat. Med.* **2012**, *18*, 1580–1586.
- Park, J. H.; Lee, S.; Kim, J. H.; Park, K.; Kim, K.; Kwon, I. C. Polymeric Nanomedicine for Cancer Therapy. *Prog. Polym. Sci.* **2008**, *33*, 113–137.
- Pan, Y.; Du, X.; Zhao, F.; Xu, B. Magnetic Nanoparticles for the Manipulation of Proteins and Cells. *Chem. Soc. Rev.* **2012**, *41*, 2912–2942.
- Ling, D.; Hyeon, T. Chemical Design of Biocompatible Iron Oxide Nanoparticles for Medical Applications. *Small* **2013**, *9*, 1450–1466.
- Nicolas, P. E. B.; Peter, J. S. Challenges for Metals in Medicine: How Nanotechnology May Help To Shape the Future. *ACS Nano* **2013**, *7*, 5654–5659.
- Xie, J.; Liu, G.; Eden, H. S.; Ai, H.; Chen, X. Surface-Engineered Magnetic Nanoparticle Platforms for Cancer Imaging and Therapy. *Acc. Chem. Res.* **2011**, *44*, 883–892.
- Owens, D. E., III; Peppas, N. A. Opsonization, Biodistribution, and Pharmacokinetics of Polymeric Nanoparticles. *Int. J. Pharm.* **2006**, *307*, 93–102.
- Fang, J.; Nakamura, H.; Maeda, H. The EPR Effect: Unique Features of Tumour Blood Vessels for Drug Delivery, Factors Involved, and Limitations and Augmentation of the Effect. *Adv. Drug Delivery Rev.* **2011**, *63*, 136–151.
- Dhar, S.; Liu, Z.; Thomale, J.; Dai, H.; Lippard, S. J. Targeted Single-Wall Carbon Nanotube-Mediated Pt (IV) Prodrug Delivery Using Folate as a Homing Device. *J. Am. Chem. Soc.* **2008**, *130*, 11467–11476.
- Zuber, G.; Zammuto-Italiano, L.; Dauty, E.; Behr, J. P. Targeted Gene Delivery to Cancer Cells: Directed Assembly of Nanometric DNA Particles Coated with Folic Acid. *Angew. Chem., Int. Ed.* **2003**, *42*, 2666–2669.
- Lee, E. S.; Na, K.; Bae, Y. H. Polymeric Micelle for Tumor pH and Folate-Mediated Targeting. *J. Controlled Release* **2003**, *91*, 103–113.
- Trédan, O.; Galmarini, C. M.; Patel, K.; Tannock, I. F. Drug Resistance and the Solid Tumour Microenvironment. *J. Natl. Cancer Inst.* **2007**, *99*, 1441–1454.
- Nichols, J. W.; Bae, Y. H. Odyssey of a Cancer Nanoparticle: From Injection Site to Site of Action. *Nano Today* **2012**, *7*, 606–618.
- Gallagher, F. A.; Kettunen, M. I.; Day, S. E.; Hu, D. E.; Ardenkjær-Larsen, J. H. Magnetic Resonance Imaging of pH *in Vivo* Using Hyperpolarized <sup>13</sup>C-Labelled Bicarbonate. *Nature* **2008**, *453*, 940–943.
- Urano, Y.; Asanuma, D.; Hama, Y.; Koyama, Y.; Barrett, T.; Kamiya, M.; Nagano, T.; Watanabe, T.; Hasegawa, A.; Choyke, P. L. Selective Molecular Imaging of Viable Cancer Cells with pH-Activatable Fluorescence Probes. *Nat. Med.* **2008**, *15*, 104–109.
- Wang, Y.; Zhou, K.; Huang, G.; Hensley, C.; Huang, X.; Ma, X.; Zhao, T.; Sumer, B. D.; DeBerardinis, R. J.; Gao, J. A Nanoparticle-Based Strategy for the Imaging of a Broad Range of Tumours by Nonlinear Amplification of Microenvironment Signals. *Nat. Mater.* **2014**, *13*, 204–212.
- Ling, D.; Park, W.; Park, S. J.; Lu, Y.; Kim, K. S.; Hackett, M. J.; Kim, B. H.; Yim, H.; Jeon, Y. S.; Na, K.; et al. Multifunctional Tumor pH-Sensitive Self-Assembled Nanoparticles for Bimodal Imaging and Treatment of Resistant Heterogeneous Tumors. *J. Am. Chem. Soc.* **2014**, *136*, 5647–5655.
- Yang, X.; Grailer, J. J.; Rowland, I. J.; Javadi, A.; Hurley, S. A.; Matson, V. Z.; Steeber, D. A.; Gong, S. Multifunctional Stable and pH-Responsive Polymer Vesicles Formed by Heterofunctional Triblock Copolymer for Targeted Anticancer Drug Delivery and Ultrasensitive MR Imaging. *ACS Nano* **2010**, *4*, 6805–6817.
- Chan, E. W.-C.; Cheng, S. C.-S.; Sin, F. W.-Y.; Xie, Y. Triptolide Induced Cytotoxic Effects on Human Promyelocytic Leukemia, T Cell Lymphoma and Human Hepatocellular Carcinoma Cell Lines. *Toxicol. Lett.* **2001**, *122*, 81–87.
- Li, Y.; Hu, S. Triptolide Sensitizes Liver Cancer Cell Lines to Chemotherapy *in Vitro* and *in Vivo*. *Panminerva Med.* **2014**, *56*, 211–220.
- Lee, E. S.; Na, K.; Bae, Y. H. Super pH-Sensitive Multifunctional Polymeric Micelle. *Nano Lett.* **2005**, *5*, 325–329.

44. Lee, E. S.; Kim, J. H.; Sim, T.; Youn, Y. S.; Lee, B.-J.; Oh, Y. T.; Oh, K. T. Feasibility Study of a pH Sensitive Nanomedicine Using Doxorubicin Loaded Poly(aspartic acid-graft-imidazole)-block-Poly(ethylene glycol) Micelles. *J. Mater. Chem. B* **2014**, *2*, 1152–1159.
45. Kang, H. C.; Bae, Y. H. Endolysosomolytically Active pH-Sensitive Polymeric Nanotechnology; *Organelle-Specific Pharmaceutical Nanotechnology*; John Wiley & Sons: New York, 2010; pp 247–262.
46. Feng, G.-S. Conflicting Roles of Molecules in Hepatocarcinogenesis: Paradigm or Paradox. *Cancer Cell* **2012**, *21*, 150–154.
47. Bard-Chapeau, E. A.; Li, S.; Ding, J.; Zhang, S. S.; Zhu, H. H.; Princen, F.; Fang, D. D.; Han, T.; Baily-Maitre, B.; Poli, V.; *et al.* *Ptpn11/Shp2* Acts as a Tumour Suppressor in Hepatocellular Carcinogenesis. *Cancer Cell* **2011**, *19*, 629–639.
48. Zhang, T.; Guo, W.; Yang, Y.; Liu, W.; Guo, L.; Gu, Y.; Shu, Y.; Wang, L.; Wu, X.; Hua, Z.; *et al.* Loss of SHP-2 Activity in CD4+ T Cells Promotes Melanoma Progression and Metastasis. *Sci. Rep.* **2013**, *3*, No. 2845; DOI: 10.1038/srep02845.
49. Xia, H.; Ooi, L. L. P. J.; Hui, K. M. MicroRNA-216a/217-induced Epithelial-Mesenchymal Transition Targets PTEN and SMAD7 To Promote Drug Resistance and Recurrence of Liver Cancer. *Hepatology* **2013**, *58*, 629–641.
50. Wang, S. M.; Ooi, L. L. P. J.; Hui, K. M. Upregulation of Rac GTPase-Activating Protein 1 is Significantly Associated with the Early Recurrence of Human Hepatocellular Carcinoma. *Clin. Cancer Res.* **2011**, *17*, 6040–6051.
51. Xia, H.; Ooi, L. L. P. J.; Hui, K. M. MiR-214 Targets  $\beta$ -Catenin Pathway To Suppress Invasion, Stem-Like Traits and Recurrence of Human Hepatocellular Carcinoma. *PLoS One* **2012**, *7*, e44206.
52. Wilder, R.; Mobashery, S. The Use of Triphosgene in Preparation of N-Carboxy- $\alpha$ -amino Acid Anhydrides. *J. Org. Chem.* **1992**, *57*, 2755–2756.
53. Lee, C.-S.; Park, W.; Park, S.-j.; Na, K. Endolysosomal Environment-Responsive Photodynamic Nanocarrier to Enhance Cytosolic Drug Delivery via Photosensitizer-mediated Membrane Disruption. *Biomaterials* **2013**, *34*, 9227–9236.
54. Park, H.; Na, K. Conjugation of the Photosensitizer Chlorin e6 to Pluronic F127 for Enhanced Cellular Internalization for Photodynamic Therapy. *Biomaterials* **2013**, *34*, 6992–7000.